Ubiquity of ferromagnetic signals in common diamagnetic oxide crystals

M. Khalid, A. Setzer, M. Ziese, and P. Esquinazi*
Division of Superconductivity and Magnetism, University of Leipzig, D-04103 Leipzig, Germany

D. Spemann
Division of Nuclear Solid State Physics, University of Leipzig, D-04103 Leipzig, Germany

A. Pöppl
Division of Magnetic Resonance of Complex Quantum Solids, University of Leipzig, D-04103 Leipzig, Germany

E. Goering
Max-Planck-Institut für Metallforschung, Heisenbergstrasse 3, D-70569 Stuttgart, Germany
(Received 2 March 2010; published 10 June 2010)

The magnetic properties of MgO, $MgAl_2O_4$, $SrTiO_3$, $LaAlO_3$, LSAT, and ZnO single crystals were investigated. These crystals show three contributions to the magnetization, namely, an intrinsic diamagnetic contribution, a paramagnetic contribution, due to various transition-metal impurities, as well as a ferromagnetic contribution. The latter shows coercive field values that are rather independent of the actual crystal material. The ferromagnetic hysteresis loops of the magnetization per volume suggest a surface contribution. The origin of the ferromagnetic contribution as arising from either defect-induced ferromagnetism or ferromagnetic impurities is discussed.

DOI: 10.1103/PhysRevB.81.214414 PACS number(s): 77.84.Bw, 75.50.Pp, 75.20.Ck, 75.70.Rf

I. INTRODUCTION

A brief report on the observation of ferromagnetic hysteresis loops in dielectric and diamagnetic HfO_2 films[1] sparked a flurry of recent research activity on defect-induced ferromagnetism in oxides.[2–6] This interesting magnetic phenomenon was actually reported before in carbon-based systems[7] and its existence recently supported by x-ray magnetic circular dichroism (XMCD) measurements at the carbon *K* edge of irradiated spots in carbon films[8] as well as in highly oriented pyrolytic graphite, as received as well as irradiated.[9] Therefore, one may expect that this defect-induced magnetism appears also in other nominally nonferromagnetic systems with *p* bands. In the case of the oxides systems under scrutiny and in their stoichiometric bulk form, all evidence to date suggests that they are diamagnetic. Most of the magnetic studies in oxides have been conducted on thin-film materials because defects occur naturally there due to either the existence of vacancies, strain relaxation near interfaces or the introduction of light, nonmagnetic elements such as hydrogen or nitrogen. In general, however, the ferromagnetic signals are tiny, in part due to the small amount of material present in a 1–100-nm-thick film, in part since the samples might be magnetically inhomogeneous with only few ferromagnetic clusters. This makes the task of the experimenter quite formidable and, as a consequence of the tiny ferromagnetic signals in the microelectromagnetic unit region, it is difficult to exclude the contribution of ferromagnetic impurities to the total signal observed. Unless one tries to characterize the impurity concentration of the samples with the best methods available and takes care of any possible sample handling artifacts, any study of this phenomenon might be thoroughly criticized in this respect as was the case of the initial report.[10] Though impurity measurements are necessary in this research field, they might not be sufficient to prove or disprove intrinsic ferromagnetism. Only systematic studies provide the necessary certainty that the observed phenomenon is or is not magnetic-impurity related. One has to acknowledge the fact that ferromagneticlike signals in certain oxides have been observed by many research groups such that not every signal can be dismissed as due to ferromagnetic impurities.

In the present work the magnetic signals from commercially available substrate crystals were investigated. On one hand, this is important as a preparatory study for the investigation of thin-film samples that are grown on just these substrates. But this study actually brings about more than a mere substrate characterization. It turns out that all substrates studied show ferromagneticlike signals and that these ferromagnetic signals share certain general features over a surprisingly broad variety of substrate compounds. The normalization of the ferromagnetic moments per sample volume (or surface area) suggests that the near-surface region may play a role in the observed magnetism; moreover, hydrogen[11–16] as well as vacancies[4,17–23] might trigger this phenomenon, as recently discussed in the literature. We expect that the results of the present work and its conclusion should have a wide validity since a literature survey reveals that most samples show saturating magnetic moments as well as coercive fields in a very narrow parameter window. Therefore the present work can serve as a reference for the identification of ferromagnetic signals in diluted magnetic semiconductors.

The experimental approach presented here is rather unique since it combines data from five techniques—high-resolution superconducting quantum interferometer device (SQUID) magnetometry, electron paramagnetic resonance (EPR), XMCD, x-ray absorption spectroscopy (XAS), and particle-induced x-ray emission (PIXE)—in the study of identical samples. Especially the very sensitive PIXE measurements assure that the impurity content is well controlled,

TABLE I. Structural and magnetic properties of the crystals studied in this work. LSAT $=(LaAlO_3)_{0.3}(Sr_2AlTaO_6)_{0.7}$.

Material	Density (g/cm^3)	Mass (mg)	Lattice constant (nm)	χ_{dia}	χ_{dia} literature values[a]
MgO	3.58	46.5	0.4212	-1.80×10^{-5}	-2.03×10^{-5}
$MgAl_2O_4$	3.60	44.6	0.8083	-1.69×10^{-5}	
$SrTiO_3$ I	5.12	61.1	0.3905	-0.65×10^{-5}	
$SrTiO_3$ II		92.4			
$LaAlO_3$ I	6.51	86.8	0.3821	-1.76×10^{-5}	
$LaAlO_3$ II		117.3			
LSAT	6.74	82.5	0.3868	-1.63×10^{-5}	
ZnO I	5.70	42.6	$a=0.325$	-2.47×10^{-5}	$-(2.2\cdots2.4)\times10^{-5}$
ZnO II		65.8	$c=0.313$		

[a]Reference 28.

as becomes clear from the comparison of the results obtained from the different magnetic characterizations.

II. EXPERIMENTAL

In this study all investigated single-crystalline substrates were obtained from Crystec GmbH, Berlin. Apart from sample ZnO II, all crystals were parallelepipeds with dimensions of either $5\times5\times0.5$ or $6\times6\times0.5$ mm^3. Crystal ZnO II was smaller and of irregular shape. For SQUID measurements a Quantum Design magnetic property measurement system (MPMS-7) SQUID equipped with the reciprocating sample option (RSO) was used. The substrates were glued with low-temperature varnish (General Electric 7031) onto rectangular glass slabs about 16 cm long. These glass slabs were mounted within the typical straws used for SQUID measurements, which in turn were attached to the carbon-fiber sample rod of the RSO system. This method of sample mounting has been previously shown to introduce no detectable ferromagnetic signals.[24]

Using the RSO the SQUID has a resolution of $\sim10^{-9}$ emu$=10^{-12}$ Am^2 at best. In all SQUID measurements presented here the magnetic field was corrected for the hysteresis of the superconducting magnet. For this the magnetic moment of a standard Pd calibration sample was measured at 300 K with the same field sequence as the oxide crystals. The actual field is obtained by assuming perfect paramagnetic behavior of the Pd sample and attributing deviations to the field hysteresis. Cycling the field from 5 T to nominally zero field yields a typical residual field of about -1.2 mT.

For PIXE measurements, the substrates were glued with low temperature varnish onto silicon wafers followed by the deposition of an approximately 10-nm-thick Au film. The gold film does not produce any ferromagnetic hysteresis, as was shown in a study of the magnetization of sapphire substrates.[25] The PIXE measurements were performed with the 2.25 MeV proton beam "LIPSION" at the University of Leipzig. Continuous-wave EPR measurements were performed at 300 K on a X-band Bruker ELEXYS E580 spectrometer operating at a microwave frequency of 9.781 GHz. We have performed XMCD and XAS measurements on $LaAlO_3$, $SrTiO_3$, and $MgAl_2O_4$ substrates at the Fe $L_{2,3}$ edges at the elliptical undulator beamline UE56/2 of the Helmholtz-Zentrum Berlin für Materialien und Energie—Storage Ring BESSY II. For more details about the experimental setup and XMCD technique see Refs. 26 and 27.

III. RESULTS AND DISCUSSION

In total four MgO, two $MgAl_2O_4$, three $LaAlO_3$, three $SrTiO_3$, three ZnO (one with a homoepitaxially grown ZnO film on top), and one $(LaAlO_3)_{0.3}(Sr_2AlTaO_6)_{0.7}$ (LSAT) substrates have been measured. Within each substrate batch, the variations in the magnetic properties and the impurity concentrations were small. Therefore only results for one substrate for each compound and substrate batch are reported. For ZnO, $SrTiO_3$, and $LaAlO_3$ results on two samples (ZnO I and II, $SrTiO_3$ I and II, and $LaAlO_3$ I and II) from different batches are shown. The ferromagnetic properties of these last samples depend on the delivered batch. An overview of the samples including density, sample mass, lattice constants, and diamagnetic susceptibility is given in Table I.

A. Magnetization: $M(T)$

Most of the magnetization values presented in this work were calculated as the measured magnetic moment divided by the sample volume, which is actually equivalent to dividing by the sample area due to the similar thickness of the substrates. In the case of ferromagnetic signals we will compare these values with the ones obtained dividing the moment by the sample mass. Especially when discussing the origin of the ferromagnetism we should not take the (extremely small) absolute values of the magnetization in the hysteresis loops as representing intrinsic magnetization values, simply because the amount of ferromagnetic mass or volume in the samples remains actually unknown.

Figure 1 shows the magnetization of six crystals as a function of (a) magnetic field at 300 K and (b) temperature at 1 T. The samples are clearly diamagnetic at room temperature with the diamagnetic susceptibilities of MgO, $MgAl_2O_4$,

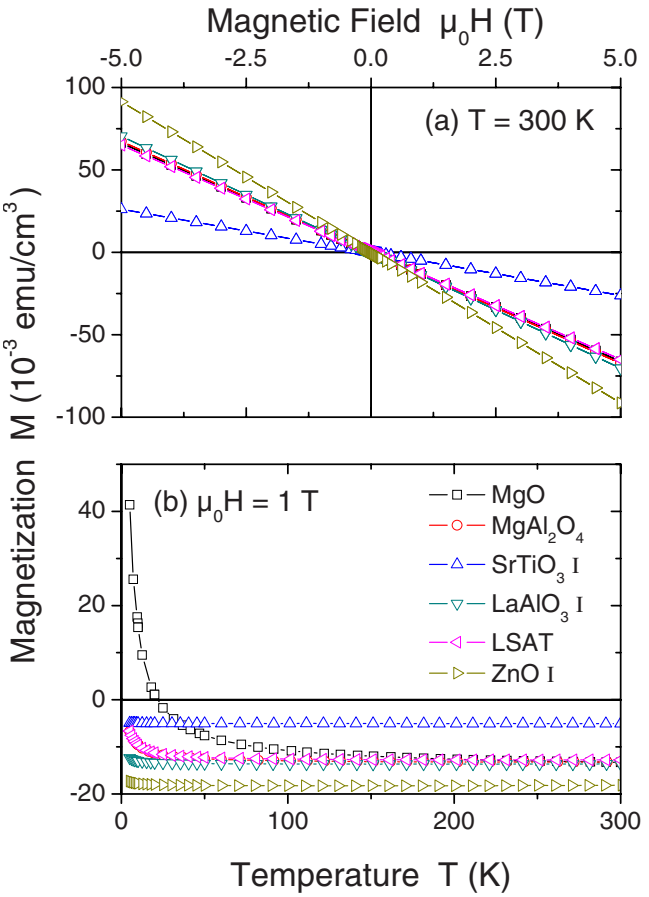

FIG. 1. (Color online) (a) Magnetization as a function of applied magnetic field at 300 K. (b) Magnetization as a function of temperature in an applied field of 1 T. Note that the magnetization of $MgAl_2O_4$ and LSAT are practically equal.

$LaAlO_3$, and LSAT being practically equal, that of $SrTiO_3$ about half of that (absolute) value and that of ZnO the highest in this group of compounds, see Table I. The rather temperature independence of the magnetization in Fig. 1(b) suggests that the $SrTiO_3$, $LaAlO_3$, and ZnO crystals are quite pure, whereas the other three crystals contain varying amounts of impurities with the MgO crystal being the most impure. This qualitative result from the magnetization measurements is well corroborated by the PIXE results, see Table II.

B. Case of MgO

Since the impurity concentration in the MgO crystal is the largest, this sample will be discussed in more detail under two aspects, namely, the consistency of magnetization and PIXE results and the magnetic behavior of the iron concentration. The PIXE analysis shows traces of Fe, Mn, Cr, V as well as 187 ± 3 μg/g Ca impurities. The latter are presumably diamagnetic (Ca^{2+}) and do not contribute to the paramagnetic response. The valence state of the paramagnetic impurities can be obtained from EPR. Figure 2 shows an EPR spectrum recorded on the MgO crystal at room temperature along the [100] direction. In the field range between 320 and 390 mT we observe a superposition of an intense manganese hyperfine (hf) sextet (lines 1) with those of a vanadium hf octet (lines 2). The spectrum is indicative of Mn_c^{2+} ions having an electron spin[29] $S=5/2$ and V_c^{2+} ions with $S=3/2$ in cubic symmetry incorporated at Mg lattice sites.[29,30] The determined Landé g factors g and metal ion hf coupling constants A are $g^{\mathrm{Mn}}=2.0021$, $A^{\mathrm{Mn}}=0.0081$ cm^{-1}, $g^{\mathrm{V}}=1.984$, and $A^{\mathrm{V}}=0.0075$ cm^{-1}. A further resonance line (3) is accompanied by four less intense hyperfine signals (lines 3′) and can be assigned to $Cr_c^{3+}(S=3/2)$ ions at Mg sites in cubic symmetry on the basis of the estimated parameters $g^{\mathrm{Cr}}=1.982$ and $A^{\mathrm{Cr}}=0.0016$ cm^{-1}.[29] A number of much less intense but sharp EPR signals (lines 4) result from minor vacancy-associated high spin $Fe_v^{3+}(S=5/2)$ and $Cr_v^{3+}(S=3/2)$ species in axial and orthorhombic symmetry.[31–34] Whereas all these EPR signals with linewidths well below 0.1 mT are due to magnetically isolated metal ions incorporated at defined lattice sites the broad resonance line (5) at about 285 mT corresponding to $g=2.45$ might indicate the additional presence of vacancies or magnetic-ion clusters in the MgO substrate single crystal.

With this information as well as with the impurity concentration an effective Curie constant can be calculated as

$$C = C_{\mathrm{Fe}} + C_{\mathrm{Mn}} + C_{\mathrm{Cr}} + C_{\mathrm{V}} \tag{1}$$

with the Curie constants of the respective impurity ions given by

$$C_I = n_I \frac{\mu_0 \mu_B^2 g_I S_I (S_I + 1)}{3 k_B}. \tag{2}$$

Here μ_0 is the vacuum permeability, μ_B the Bohr magneton, and k_B the Boltzmann constant. The impurity concentration n_I can be obtained from

TABLE II. Results of the PIXE analysis. The concentrations are given in units of microgram element per gram oxide compound. Numbers in brackets are the detection limit.

Material	V μg/g	Cr μg/g	Mn μg/g	Fe μg/g	Co μg/g	Ni μg/g
MgO	35(1)	27(1)	13(1)	88(1)		1(1)
$MgAl_2O_4$			4(1)	14(2)		
$SrTiO_3$ I				4(4)	7(4)	(7)
$LaAlO_3$ I				(50)	13(9)	(13)
LSAT				(100)	20(50)	61(14)
ZnO I				6(6)		13(13)

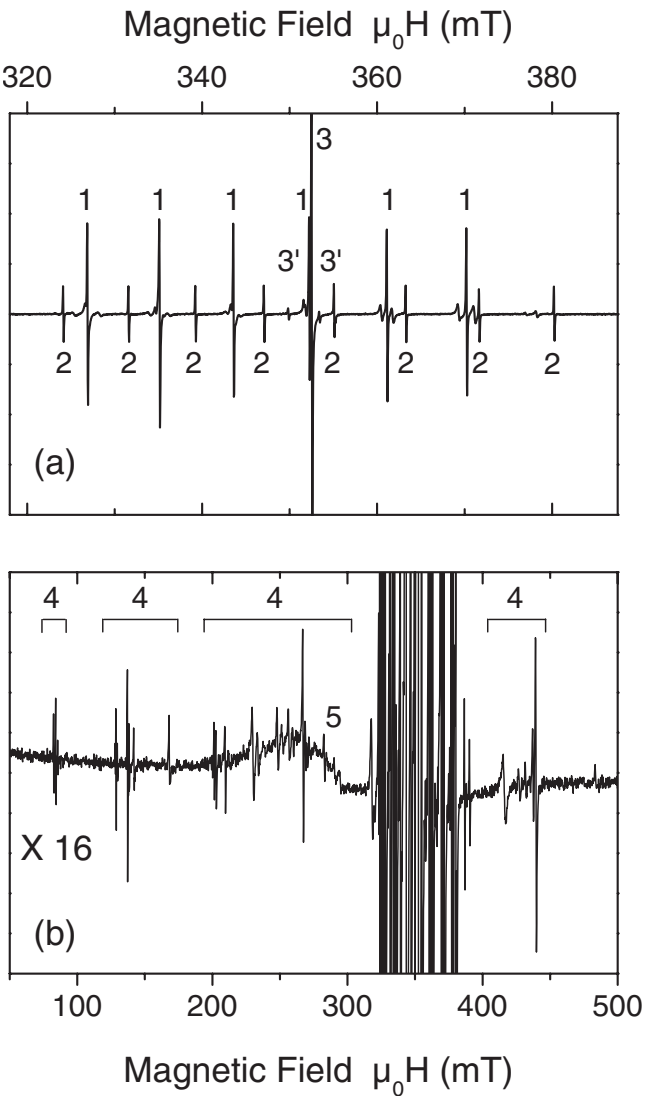

FIG. 2. EPR spectrum of MgO at 300 K in (a) a narrow field and (b) a wider field range at higher receiver gain. The EPR lines labeled 1, 2, 3, and 3′ indicate Mn_c^{2+}, Cr_c^{3+}, and V_c^{2+} ions on undisturbed cubic Mg sites. (b) Lines 4 are due to vacancy associated Fe_v^{3+} and Cr_v^{3+} ions. The origin of the wide bump, signal 5, between 200 and 300 mT is actually unknown; it might be caused by either vacancies or metal ion clusters.

$$n_I = \rho_{\mathrm{MgO}} c_I \frac{N_A}{M_I}, \tag{3}$$

where c_I is the impurity concentration as measured by PIXE, ρ_{MgO} the density of MgO, N_A Avogadro's constant, and M_I the molar mass of the respective ion. This yields the following concentrations: Fe: 3.4×10^{24} m^{-3}, Mn: 5.1×10^{23} m^{-3}, Cr: 1.1×10^{24} m^{-3}, and V: 1.5×10^{24} m^{-3}. The effective Curie constant is obtained as $C=4.6\times10^{-4}$ K.

Figure 3(a) shows the inverse susceptibility of the MgO crystal corrected by the diamagnetic contribution as a function of temperature. Below 150 K this is clearly linear in temperature yielding a Curie constant $C=(4.4\pm0.2)\times10^{-4}$ K from

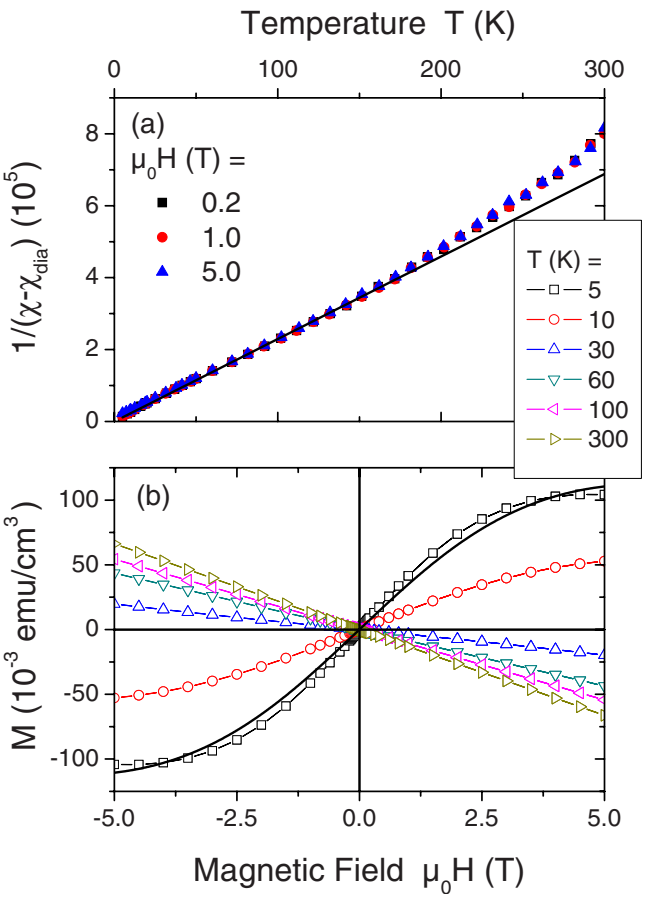

FIG. 3. (Color online) (a) Inverse susceptibility $1/(\chi-\chi_{dia})$ of the MgO crystal measured at various magnetic fields and corrected for the diamagnetic susceptibility. The solid line is a fit to the data below 150 K. Note that, for simplicity, we subtracted from the data a temperature-independent value χ_{dia}. Therefore, the deviation of the data from the $1/T$ curve at $T>200$ K may be due to the temperature dependence of the diamagnetic contribution, which is not known with certainty. (b) Magnetization curves of the MgO crystal at various temperatures. The solid line was calculated from the concentrations and angular momentum values of the Fe, Mn, Cr, and V impurities without any adjustable parameters, see text for further details.

$$\chi - \chi_{dia} = \frac{C}{T}. \tag{4}$$

This value is in excellent agreement with the value derived from the impurity concentrations as determined by PIXE and the valence states as determined by EPR. This clearly shows that impurity-concentration determinations from magnetic and PIXE measurements are complementary. Moreover, the comparison shows that the overwhelming fraction, if not all, of the iron impurities in the MgO sample are paramagnetic.

Figure 3(b) shows magnetization curves for the MgO crystal recorded at various temperatures. The paramagnetic contribution becomes more pronounced with decreasing temperature. The solid line in Fig. 3(b) was calculated from the measured impurity concentrations and the aforementioned values of the angular momenta using the expression

$$M = \sum_I M_{SI} B_{S_I}\left(\frac{g_I S_I \mu_B \mu_0 H}{k_B T}\right) + \chi_{dia} H \tag{5}$$

with the saturation magnetization $M_{SI}=n_I g_I S_I \mu_B$ of the respective paramagnetic impurities and the Brillouin function,

$$B_S(x) = \frac{2S+1}{2S}\coth\left(\frac{2S+1}{2S}x\right) - \frac{1}{2S}\coth\left(\frac{x}{2S}\right), \tag{6}$$

$x=gS\mu_B B/k_B T$. The agreement with the measured data at 5 K is excellent, taking into account that no free parameter was used.

To summarize this analysis we note two main conclusions: (1) the impurity concentrations measured by PIXE allow for a detailed prediction of the paramagnetic response of the crystal and (2) the major part of the impurities occupies Mg sites and is not ferromagnetically ordered.

C. Magnetization hysteresis: $M(H)$

The results presented up to this point constitute a nice illustration for the use of the three complementary techniques SQUID magnetometry, PIXE, and EPR, but are not *per se* astonishing. If the samples do only show intrinsic diamagnetic and impurity related paramagnetic response, a subtraction of a straight line from the data at 300 K, see Fig. 3(b), should yield white noise. This, however, is not the case. Figure 4 shows the residual response ΔM (per sample mass) of six crystals after subtraction of the diamagnetic and paramagnetic contributions,

$$\Delta M = M - M_{para} - M_{dia}. \tag{7}$$

This residual response ΔM has a clear ferromagnetic character with well-defined coercive field and remanent magnetization. The virgin branch of the curves is not shown in Fig. 4 but can be clearly observed as shown in Fig. 5(b) for $SrTiO_3$. Note that the MgO crystal with the largest Fe impurity concentration has the smallest ferromagnetic contribution.

Figure 5 shows the temperature dependence of the ferromagnetic contribution for the $SrTiO_3$ crystal. The saturation magnetization is rather temperature independent at least up to 300 K, see Fig. 5(a), within the error limits set by the correction for the paramagnetic contribution at low temperatures. This is valid for all the crystals studied here.

The remanent magnetization M_{rem} and coercive field H_c of the ferromagnetic contribution were determined and are shown in Fig. 6. The remanent magnetization is chosen to characterize the magnetic response of the crystals, since it does not change when correcting the measured data for paramagnetic and diamagnetic contributions, in contrast to the coercive fields values.

The temperature dependence of the remanent magnetization as well as the coercive field are quite similar for all the crystals studied. Apart from the MgO crystal the remanent magnetization varies by a factor of 2 at most between the different samples, see Fig. 6(a). The saturation magnetization of all crystals is rather independent of temperature within experimental error and is listed in Table III.

Note that all the magnetization values presented in Fig. 4 are—after subtraction of the paramagnetic and diamagnetic

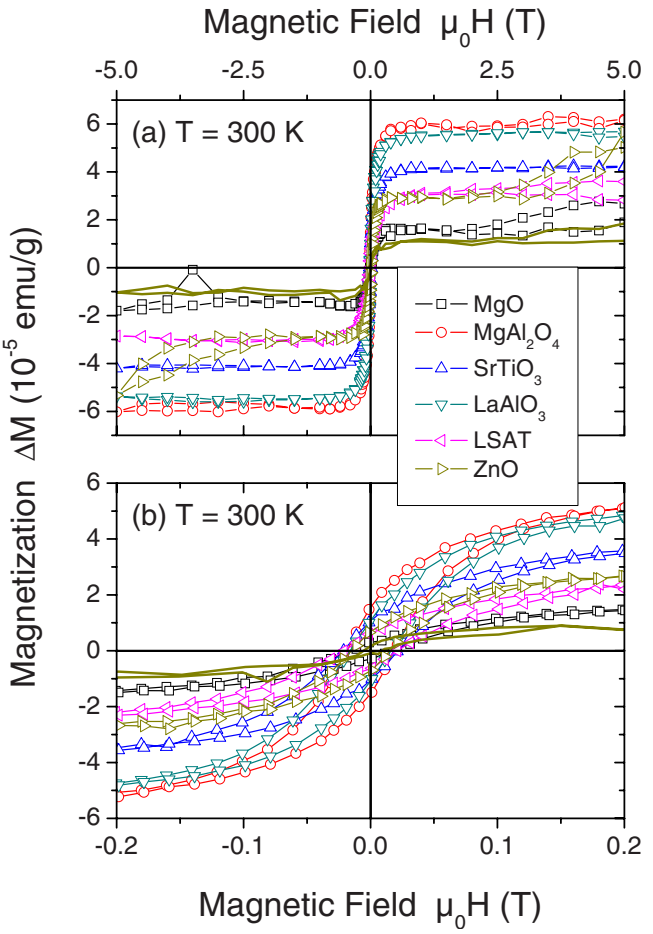

FIG. 4. (Color online) Ferromagneticlike contribution to the magnetization of the diamagnetic crystals at 300 K in (a) a wide and (b) a narrow field range. The continuous line corresponds to the ZnO II substrate from a different batch.

signals, see Eq. (7)—the ferromagnetic moment per sample mass, assuming that the whole sample mass is ferromagnetic. This is the reason why those magnetization values are so small and probably meaningless. It is unrealistic to believe that a ferromagnetic phase that remains robust above 300 K can have a magnetization on the order of 10^{-5} emu/g; compare this value with the magnetization $\gtrsim 50$ emu/g that usual ferromagnets with $T_C \gtrsim 300$ K have. Because this unrealistic "ferromagnetic mass" assumption is usually done in the literature and to get a feeling for the calculated magnitude of the saturation magnetization, we estimated the equivalent Fe-impurity concentrations it implies. Let us assume that it is produced by ferromagnetically ordered magnetic moments with a total angular momentum $S=5/2$ and a g factor $g=2$. Then the density of these ions can be estimated as

$$n_F = \frac{M_{SF}}{gS\mu_B} \tag{8}$$

and can be converted into an equivalent iron impurity concentration using

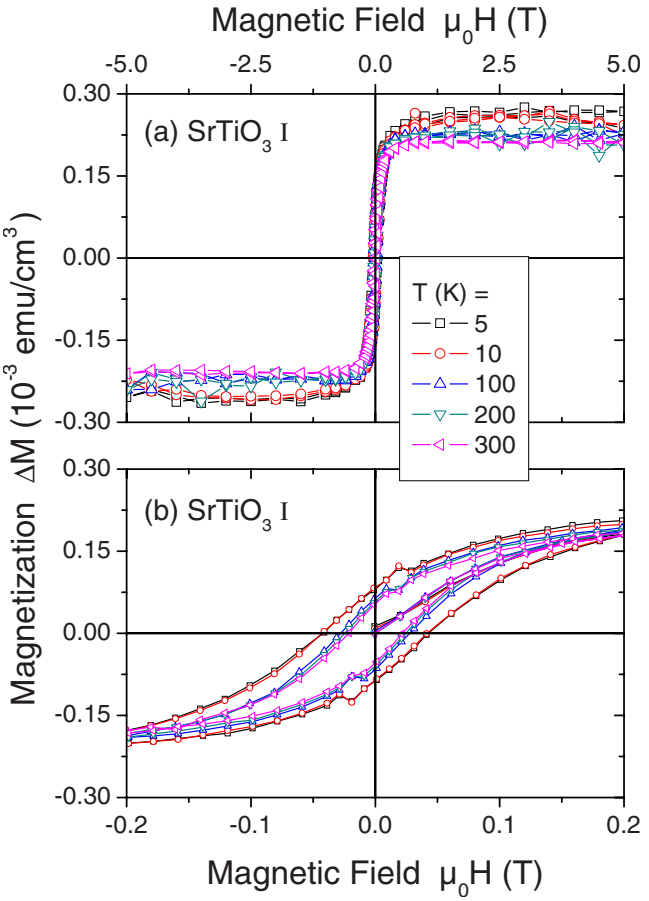

FIG. 5. (Color online) Ferromagneticlike contribution to the magnetization of the $SrTiO_3$ crystal in (a) a wide and (b) a narrow field range and at various temperatures.

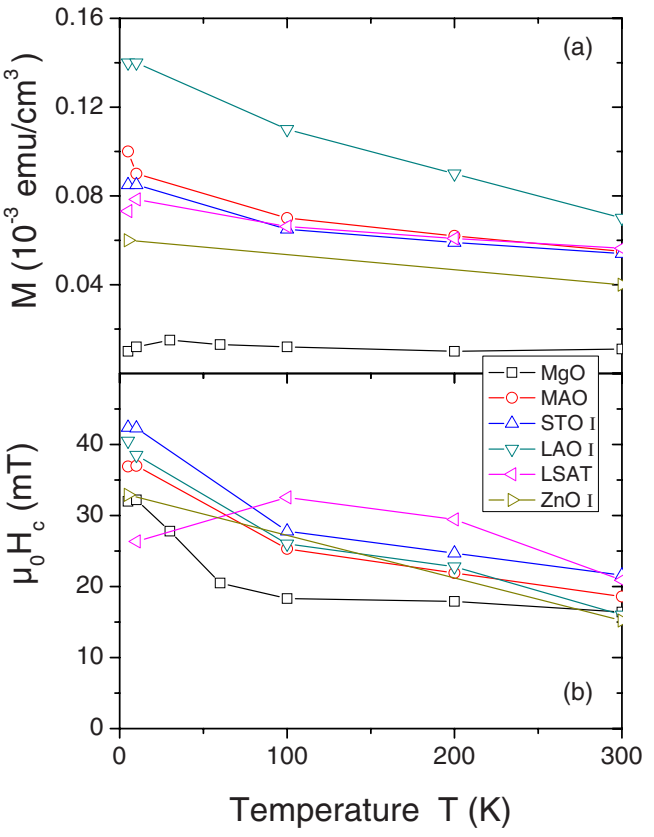

FIG. 6. (Color online) (a) Remanent magnetization and (b) coercive field determined from the ferromagnetic signal.

$$n_{F,\mathrm{Fe}} = \frac{n_F M_{\mathrm{Fe}}}{N_A \rho}, \tag{9}$$

where M_{Fe} (in grams per mole) is the molar mass of iron and ρ is the density of the respective substrate. The corresponding values are listed in Table III. For comparison the saturation magnetization M_{SP} of the paramagnetic component as estimated from the hysteresis loops at 5 K is also included in Table III along with the density of paramagnetic ions and the equivalent iron ion concentration. The ferromagnetic equivalent iron-impurity concentration is much smaller ($\lesssim 1\%$) than the paramagnetic equivalent iron-impurity concentration. Actually, the ferromagnetic magnetization component is so small that—if assumed to be uniformly distributed through the samples—it would lead to an internal field $\mu_0 H_{int} \simeq \mu_0 M_{SF} < 5 \times 10^{-4}$ mT, far below the linewidth observed in the EPR measurements.

Which are the characteristics and what is the origin of this ferromagnetic contribution? It is characterized by a small saturation magnetization value (if one takes the whole sample mass or sample volume), by a high Curie temperature far above room temperature, and by a striking independence of coercive field (and within a factor of 5 also of the remanent magnetization) of the actual chemical composition of the compound. It is not generated by the residual field artifact since this has been corrected for. A possible hint on the origin of the ferromagnetic signals is obtained when we calculate the magnetization taking into account the sample volume (or its surface since the thickness of the samples is identical) instead of the sample mass. Figure 7 shows the ferromagnetic part of the volume magnetization of the substrates at 300 K. In contrast to the mass magnetization, see Fig. 4, quantitatively similar hysteresis loops are obtained for four of the substrates, whereas clear deviations are observed for MgO, which coincides with the ZnO II substrate and $LaAlO_3$ substrates, see Fig. 7. This result suggests that probably the ferromagnetic region is concentrated mainly at the surface or at the near-surface region. Assuming a near-surface region of thickness d_s as the ferromagnetic one, the measure magnetization values have to be rescaled by $2d/d_s$, where $d=0.5$ mm is the substrate crystal thickness. Assuming near-surface layer thicknesses of 10 and 1 nm, the surface magnetization values are estimated to be five or six orders of magnitude larger than those shown in Fig. 4, i.e., in the range between 6 and 60 emu/g.

Before discussing further evidence that indicates that at least in some of the crystals the surface may play a mayor role in the ferromagnetic signal, we would like to provide here some simple estimates. Several works claimed that the unexpected ferromagnetism in several oxides stems from oxygen vacancies.[1,5,6,35–37] Therefore, let us assume that oxygen vacancies produce unpaired spins and probably oxygen vacancy clusters with some ferromagnetic ordering. If these vacancies are only localized at the surfaces, then an areal

TABLE III. Saturation magnetization obtained from the ferromagnetic hysteresis loops M_{SF}, equivalent paramagnetic saturation M_{SP} obtained from the hysteresis loops at 5 K, density n_F, n_P and equivalent Fe-impurity concentration $n_{\mathrm{Fe},F}$, $n_{\mathrm{Fe},P}$ of the ferromagnetic and paramagnetic contribution, respectively, obtained under the assumption that the whole sample mass contributes to the ferromagnetic signal. Note the differences in the equivalent Fe-impurity concentration obtained for samples from different batches.

Material	M_{SF} 10^{-3} emu/cm^3	n_F 10^{21} m^{-3}	$n_{F,\mathrm{Fe}}$ μg/g	M_{SP} 10^{-3} emu/cm^3	n_P 10^{21} m^{-3}	$n_{P,\mathrm{Fe}}$ μg/g
MgO	0.06	1.3	0.03	215	4600	120
$MgAl_2O_4$	0.23	5.0	0.13	22	470	12
$SrTiO_3$ I	0.24	5.2	0.09	0.25	5.4	0.10
$SrTiO_3$ II	0.03	0.7	0.01			
$LaAlO_3$ I	0.38	8.2	0.12	4.5	97	1.4
$LaAlO_3$ II	0.04	0.9	0.01			
LSAT	0.23	5.0	0.07	19	415	5.7
ZnO I	0.16	3.5	0.06	3.1	66	1.1
ZnO II	0.06	1.3	0.02			

spin density of about 5×10^4 $\mu_B/(\mathrm{nm})^2$ results for a typical saturation magnetization of 2×10^3 A/m$\sim$4 emu/g. This areal spin density value is one order of magnitude larger than the areal spin densities of 100–400 $\mu_B/(\mathrm{nm})^2$ reported in Ref. 38. This indicates that not all the ferromagnetic signal comes from the surface itself but from the near-surface region, e.g., within 10 nm inside the sample volume if we take as reference the values in Ref. 38. We note, however, that there is actually no clear experimental evidence that oxygen vacancies are the origin of the defect-induced magnetic order in these oxides. In contrast, experimental evidence for the role of cation vacancies, as in the case of ZnO (Refs. 36 and 39) or MgO,[17,40] already exists as well as first-principles calculations that demonstrate that cation and not oxygen vacancies trigger the magnetic order in several oxides such as in ZnO,[18,19] MgO,[17,20,41] HfO_2, TiO_2, SnO_2, and ZrO_2,[4,21–23,41,42] although it was also shown that light element impurities might sustain a magnetic moment, but probably no ferromagnetic order.[43–45] Even in this case the estimate above remains valid.

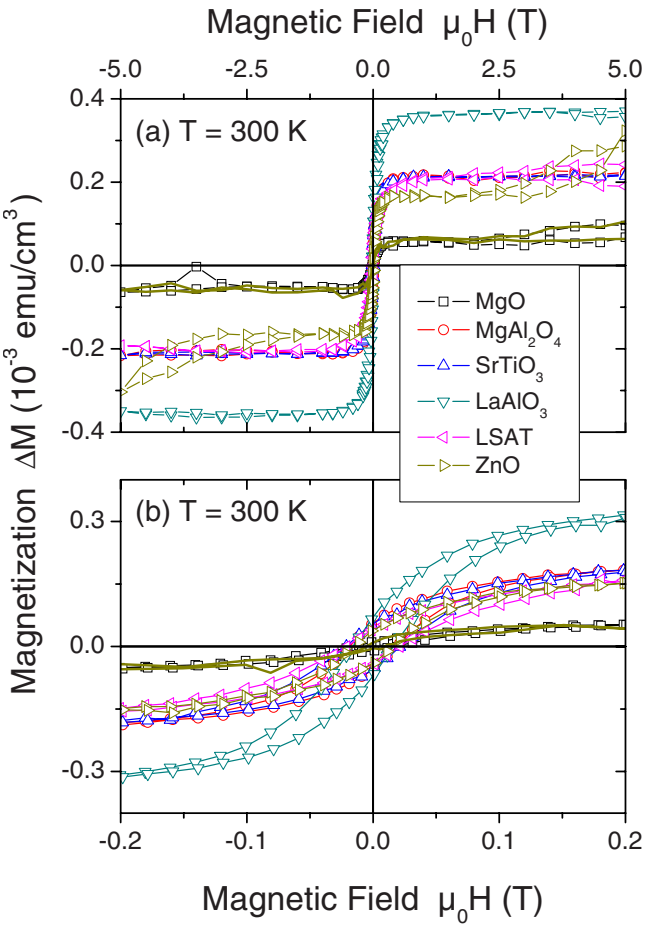

FIG. 7. (Color online) Volume magnetization of the ferromagneticlike contribution to the magnetization of the crystals at 300 K in (a) a wide and (b) a narrow field range. The continuous line corresponds to the ZnO II substrate.

On the other hand, one has to consider the growth, cutting, and polishing procedures used to fabricate the substrate crystals. Since these are largely identical for all samples studied here, it would not be astonishing to find a similar density of ferromagnetic, probably iron-based cluster impurities. Although the EPR measurements may indicate the presence of magnetic metal ion clusters in MgO, see Fig. 2, there was no similar evidence for the existence of metallic clusters in $MgAl_2O_4$ and $SrTiO_3$, for example.

In order to estimate the size of nanoparticles with a stable magnetization at room temperature we proceed with the following simple argument. For iron the cubic magnetocrystalline anisotropy constant is $K_1=4.8\times10^4$ J/m^3 at room temperature. Using a blocking temperature criterion $K_1V=25k_BT$ one obtains the radius of an iron nanoparticle with blocked magnetization at room temperature as

$$r=\left(\frac{75k_BT}{4\pi K_1}\right)^{1/3}=8\ \mathrm{nm}. \tag{10}$$

The measured magnetic moment is typically $m_s\sim3\times10^{-9}$ Am^2. With a saturation magnetization of 2.2 T this

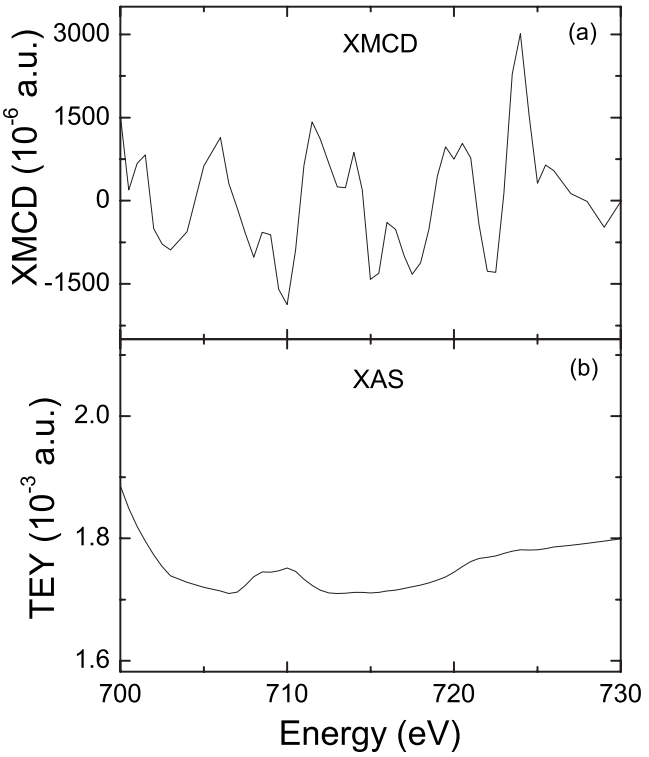

FIG. 8. (a) XMCD and (b) XAS spectra of the $LaAlO_3$ I substrate with the largest ferromagnetic magnetization contribution, see Fig. 9, at the Fe $L_{2,3}$ edges at 300 K measured at 120 mT. There is no significant XMCD signal larger than the noise, which is in the order of 1.5×10^{-3} with respect of the XAS signal, indicating the absence of ferromagnetic iron in the system.

corresponds to an iron volume of 1.4×10^{-15} m^3, i.e., about 10^9 clusters. If these clusters would be distributed throughout the 10 nm near-surface region of volume $\sim10^{-13}$ m^3, this Fe concentration is large enough to be seen by PIXE and dichroism measurements.

D. X-ray magnetic circular dichroism measurements

Further proof for the absence of ferromagnetic Fe^{3+} is obtained by XMCD, which has been used in the more surface-sensitive total electron yield mode and in the bulk sensitive total fluorescence yield mode. To measure the element-specific XMCD spectra and site-specific x-ray magnetic reflectivity, a polarized x-ray source with tunable energy and polarization in the soft x-ray range (<2 keV) is required. For XMCD measurements the beam is circularly polarized and synchrotron radiation is used as the optimal photon source, which fulfills the necessary requirements.

The circular dichroic and nonmagnetic absorption spectra of $LaAlO_3$ I, the substrate with the largest volume magnetization (see Fig. 7), are shown in Fig. 8. In case of Fe at the L_3 and L_2 edges, the strong absorption peaks are expected at photon energies of 713.6 eV and 715.2 eV, respectively.[46,47] We observed a very small Fe $L_{2,3}$-edge XAS signal on a large background. The size of the XAS fits roughly the amount of Fe detected so far. Nevertheless, the noise level of the XMCD signal, nearly three orders of magnitude smaller compared to XAS, indicates clearly the absence of ferromagnetic Fe. We conclude that XMCD and XAS measurements performed on all above-mentioned substrates did not show any significant ferromagnetic contribution and therefore it appears that Fe impurities are not the source of the ferromagnetic contribution in the measured substrates.

E. Influence of surface cleaning and etching on the magnetic properties of oxides substrates

It was recently reported that HNO_3 etching reduced or removed the ferromagnetic signal from Al_2O_3 substrates.[25,48] This result suggests that ferromagnetic metallic grains at the surface could be the origin for the measured ferromagnetism. However, as we described above, if the main part of the impurities were at the near-surface region, our analysis methods should have been able to detect these. We have also studied the effect of surface cleaning on the magnetic properties of MgO, $MgAl_2O_4$, $SrTiO_3$, $LaAlO_3$, LSAT, and ZnO substrates. For this purpose all the substrates were cleaned ultrasonically in 99.999% pure ethanol or acetone; further the $LaAlO_3$ substrates were etched in HNO_3 for various durations between 1 and 96 h. The ultrasonic cleaning time in acetone or ethanol for each sample was about 40 min. The magnetic properties of all the substrates were measured before and after the surface treatment.

Figure 9(a) shows the ferromagnetic part of the magnetization of the as-received $LaAlO_3$ II substrate and after ultrasonic cleaning in ethanol or acetone measured at 300 K. We did not observe any difference in the magnetic response of the $LaAlO_3$ II sample before and after cleaning in acetone and ethanol solutions. This substrate was etched 96 h in HNO_3 without producing any change in the ferromagnetic signal. Figure 9(b) shows the magnetization of the $LaAlO_3$ I substrate after etching with HNO_3 for durations between 1 and 90 h. A clear effect on the magnetization of the $LaAlO_3$ I substrate is observed. A small increase in the ferromagnetic magnetization appears after 1 h etching, an effect that is rather unlikely to happen if metallic impurities at the surface were the reason for its ferromagnetism. For larger etching times, however, the ferromagnetic signal decreases. This nonmonotonic behavior was reproducible in other untreated $LaAlO_3$ substrates from the same batch.

We have observed also a nonsimple change in the ferromagnetic response of the $SrTiO_3$ II substrate after ultrasonic cleaning in ethanol and acetone solutions, see Fig. 10. The ferromagneticlike response of the $SrTiO_3$ I substrate is enhanced after ultrasonic cleaning in ethanol. This behavior is reproducible for other $SrTiO_3$ substrates. When cleaned with acetone, however, the ferromagnetic response tends to vanish, see Fig. 10(a). The behavior of the total magnetic moment as a function of temperature shown in Fig. 10(b) indicates a decrease in the diamagnetic response after ethanol cleaning, whereas it increases after acetone cleaning, in qualitative agreement with the behavior of the hysteresis loops.

This switching on-off behavior of the magnetization might be due to the complex surface structure of the $SrTiO_3$ compound. The $SrTiO_3$ compound has perovskite crystal

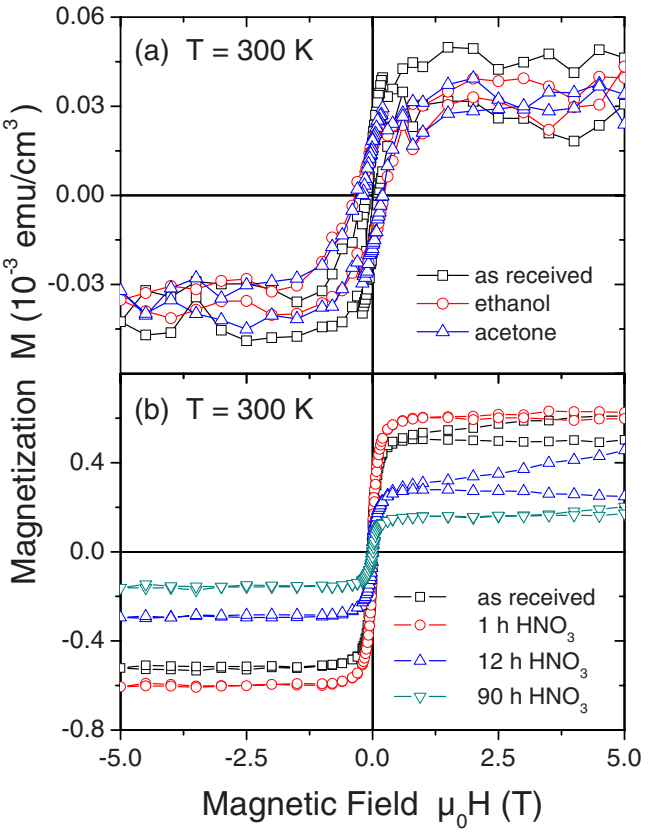

FIG. 9. (Color online) (a) Hysteresis loops of substrate $LaAlO_3$ II before and after ultrasonic cleaning in ethanol and acetone, measured at 300 K after subtraction of the diamagnetic contribution. (b) Hysteresis loops of substrate $LaAlO_3$ I before and after etching for different duration in HNO_3. Note the slight increase in the M_{SF} after the first etching procedure. The opening of the hysteresis loops at the positive field quadrant is due to a small temperature drift of the SQUID.

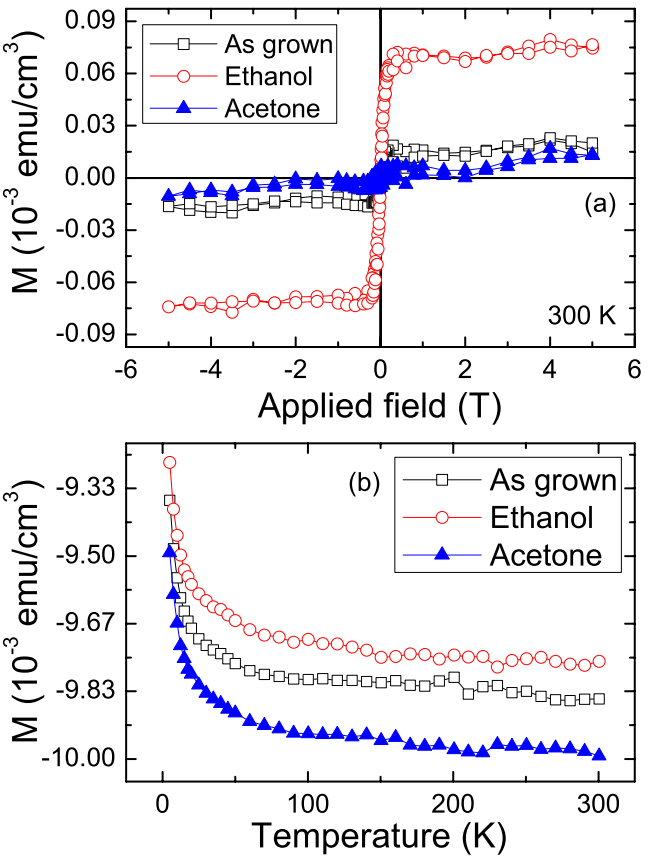

FIG. 10. (Color online) (a) Hysteresis loops at 300 K of substrate $SrTiO_3$ II in the as-received state and after cleaning in ethanol and acetone; the diamagnetic contribution was subtracted. (b) Temperature dependence of the total magnetic moment of the same sample.

structure and consisted of two nonpolar atomic planes, i.e., SrO and TiO_2, alternating along the [001] direction. The electronic and magnetic properties of $SrTiO_3$ substrate strongly depend on its termination, which can be either the SrO or TiO_2 plane.[49,50] At first glance and if one starts first with acetone cleaning, the observed decrease in the ferromagnetic moment observed after ultrasonic cleaning appears to be related to the removal of loose magnetic particles from the $SrTiO_3$ surface as already reported in other systems.[51] But this possibility can be ruled out because the ferromagneticlike moment increases again by treating it in ethanol after cleaning it with acetone, see Fig. 10.

We may speculate that the used liquids react with either Sr or Ti atoms (depending on whether the terminated surface is SrO or TiO_2) at the top layer, leaving a different electronic structure that does support the formation of the magnetic order between spins of the free oxygen bonds. On the other hand, this reaction may well be influenced by possible defects that exist or remain at the surface or near-surface region in the oxide system (point defects, vacancies, interstitials, etc.) to explain the enhancement of the ferromagnetic moment in $SrTiO_3$ at room temperature observed after ultrasonic cleaning in ethanol. As pointed out in Ref. 18, unlike O vacancies cation vacancies may prefer to cluster and reside in the near-surface region of some of these oxides. Therefore one may expect some change in their magnetic properties if the influence of these defects is modified by certain solutions.

As noted in Sec. I, nowadays attention is also focused on hydrogen-mediated ferromagnetism in oxides.[11–14] We note that clear evidence of the hydrogen influence on the magnetic order at the near-surface region of graphite has been obtained recently by XMCD measurements.[9] Hydrogen is a very reactive element and its role is different in different media. Atomic hydrogen can act either as donor or acceptor and can occupy different lattice sites and consequently modify the host structure. In general the presence of hydrogen in oxide systems can also influence the conductivity of the system.[11,52] Therefore, we may speculate that the observed ferromagnetism in $SrTiO_3$ is affected by the hydrogen content at the surface of the sample, content that might be changed by the used cleaning solution. Ultrasonic cleaning with ethanol and acetone has no effect on MgO, $MgAl_2O_4$, LSAT, and ZnO substrates.

Since the ferromagnetic signals of the substrates are always rather small due to the small ferromagnetic mass, the expected changes in the magnetization produced by surface treatments—whatever origin—will be obviously smaller.

Any further systematic work requires the characterization of surface states to bring more light on this interesting issue.

IV. CONCLUSIONS

The analysis of the magnetic response of single crystals of six different, nominally diamagnetic oxide compounds showed that three contributions, a diamagnetic, a paramagnetic, and a ferromagnetic one are present in the magnetization signals. The diamagnetic one is intrinsic, the paramagnetic contribution is mainly due to magnetic ions occupying lattice sites with impurity concentration in the 1–100 ppm range and the ferromagnetic signal is equivalent to an iron concentration *per total sample mass* in the subparts per million range. The whole systematic study done in this work, however, does not provide any direct evidence that speaks for a ferromagnetic contribution due to magnetic impurities. The ferromagnetic contribution shows some universality with respect to Curie temperature that is far above room temperature as well as temperature dependence of coercive field and to some extent also in the remanent magnetization. This universality indicates some universal origin. The available results suggest that the ferromagnetic mass might be mostly concentrated in the near-surface region, probably related to specific lattice defects and/or hydrogen influence. Future XMCD measurements checking especially the near-surface region and the oxygen $2p$ band response might help to clarify further the origin of these ferromagnetic signals.

ACKNOWLEDGMENTS

We thank B. Zada and W. Mahler for the assistance during the beam time at the undulator beam line UE56-2 at the Helmholz Zentrum Berlin (BESSY II). This work was supported by the DFG within the Collaborative Research Center (Grant No. SFB 762) "Functionality of Oxide Interfaces."

*esquin@physik.uni-leipzig.de

[1] M. Venkatesan, C. B. Fitzgerald, and J. M. D. Coey, Nature (London) **430**, 630 (2004).
[2] J. M. D. Coey, M. Venkatesan, P. Stamenov, C. B. Fitzgerald, and L. S. Dorneles, Phys. Rev. B **72**, 024450 (2005).
[3] J. M. D. Coey, M. Venkatesan, and C. B. Fitzgerald, Nature Mater. **4**, 173 (2005).
[4] C. Das Pemmaraju and S. Sanvito, Phys. Rev. Lett. **94**, 217205 (2005).
[5] A. Sundaresan, R. Bhargavi, N. Rangarajan, U. Siddesh, and C. N. R. Rao, Phys. Rev. B **74**, 161306(R) (2006).
[6] N. H. Hong, J. Sakai, N. Poirot, and V. Brizé, Phys. Rev. B **73**, 132404 (2006).
[7] P. Esquinazi, *Handbook of Magnetism and Advanced Magnetic Materials* (Wiley, Chichester, UK, 2007), pp. 2256–2281.
[8] H. Ohldag, T. Tyliszczak, R. Höhne, D. Spemann, P. Esquinazi, M. Ungureanu, and T. Butz, Phys. Rev. Lett. **98**, 187204 (2007).
[9] H. Ohldag, P. Esquinazi, E. Arenholz, D. Spemann, M. Rothermel, A. Setzer, and T. Butz, arXiv:0905.4315 (unpublished).
[10] D. W. Abraham, M. M. Frank, and S. Guha, Appl. Phys. Lett. **87**, 252502 (2005).
[11] N. Sanchez, S. Gallego, J. Cerda, and M. C. Muñoz, Phys. Rev. B **81**, 115301 (2010).
[12] L. Liu, J. Kang, Y. Wang, X. Zhang, and R. Han, Jpn. J. Appl. Phys. **47**, 8787 (2008).
[13] C. H. Park and D. J. Chadi, Phys. Rev. Lett. **94**, 127204 (2005).
[14] C. Wang, G. Zhou, J. Li, B. Yan, and W. Duan, Phys. Rev. B **77**, 245303 (2008).
[15] T. Tietze, M. Gacic, G. Schütz, G. Jakob, S. Brück, and E. Goering, New J. Phys. **10**, 055009 (2008).
[16] B. Straumal, A. A. Mazilkin, S. G. Protasova, A. A. Myatiev, P. Straumal, G. Schütz, P. van Aken, E. Goering, and B. Baretzky, Phys. Rev. B **79**, 205206 (2009).
[17] J. I. Beltrán, C. Monty, L. Balcells, and C. Martínez-Boubeta, Solid State Commun. **149**, 1654 (2009).
[18] Q. Wang, Q. Sun, G. Chen, Y. Kawazoe, and P. Jena, Phys. Rev. B **77**, 205411 (2008).
[19] D. Kim, J.-H. Yang, and J. Hong, J. Appl. Phys. **106**, 013908 (2009).
[20] F. Gao, J. Hu, C. Yang, Y. Zheng, H. Qin, L. Sun, X. Kong, and M. Jiang, Solid State Commun. **149**, 855 (2009).
[21] Y. Bai and Q. Chen, Phys. Status Solidi (RRL) **2**, 25 (2008).
[22] G. Rahman, V. M. García-Suárez, and S. C. Hong, Phys. Rev. B **78**, 184404 (2008).
[23] E. Máca, J. Kudrnovský, V. Drchal, and G. Bouzerar, Appl. Phys. Lett. **92**, 212503 (2008).
[24] J. Barzola-Quiquia, P. Esquinazi, M. Rothermel, D. Spemann, T. Butz, and N. García, Phys. Rev. B **76**, 161403(R) (2007).
[25] R. Salzer, D. Spemann, P. Esquinazi, R. Höhne, A. Setzer, K. Schindler, H. Schmidt, and T. Butz, J. Magn. Magn. Mater. **317**, 53 (2007).
[26] E. Goering, S. Gold, A. Bayer, and G. Schuetz, J. Synchrotron Radiat. **8**, 434 (2001).
[27] S. Brück, S. Bauknecht, B. Ludescher, E. Goering, and G. Schütz, Rev. Sci. Instrum. **79**, 083109 (2008).
[28] *CRC Handbook of Chemistry and Physics*, 80th ed. (CRC Press LLC, Boca Raton, London, New York, Washington, DC, 1999), pp. 4–136.
[29] W. Low and E. L. Offenbacher, *Solid State Physics* (Academic Press, New York, 1965), p. 135.
[30] W. Low, Phys. Rev. **105**, 793 (1957).
[31] J. E. Wertz and P. Auzins, Phys. Rev. **106**, 484 (1957).
[32] K. P. O'Donnell, M. O. Henry, B. Henderson, and D. O'Connell, J. Phys. C **10**, 3877 (1977).
[33] B. Henderson, J. E. Wertz, T. P. P. Hall, and R. D. Dowsing, J. Phys. C **4**, 107 (1971).
[34] R. S. de Biasi and A. Caldas, J. Phys. C **10**, 107 (1977).
[35] S. D. Yoon, Y. Chen, A. Yang, T. L. Goodrich, X. Zuo, D. A. Arena, K. Ziemer, C. Vittoria, and V. G. Harris, J. Phys.: Condens. Matter **18**, L355 (2006).
[36] N. H. Hong, J. Sakai, and V. Brizé, J. Phys.: Condens. Matter **19**, 036219 (2007).
[37] N. H. Hong, N. Poirot, and J. Sakai, Phys. Rev. B **77**, 033205 (2008).

[38] J. M. D. Coey, J. Appl. Phys. **97**, 10D313 (2005).
[39] M. Khalid, M. Ziese, A. Setzer, P. Esquinazi, M. Lorenz, H. Hochmuth, M. Grundmann, D. Spemann, T. Butz, G. Brauer, W. Anwand, G. Fischer, W. A. Adeagbo, W. Hergert, and A. Ernst, Phys. Rev. B **80**, 035331 (2009).
[40] J. F. Hu, Z. L. Zhang, M. Zhao, H. W. Qin, and M. H. Jiang, Appl. Phys. Lett. **93**, 192503 (2008).
[41] S. Gallego, J. I. Beltrán, J. Cerdá, and M. C. Muñoz, J. Phys.: Condens. Matter **17**, L451 (2005).
[42] T. Chanier, I. Opahle, M. Sargolzaei, R. Hayn, and M. Lannoo, Phys. Rev. Lett. **100**, 026405 (2008).
[43] A. Droghetti, C. D. Pemmaraju, and S. Sanvito, Phys. Rev. B **78**, 140404(R) (2008).
[44] V. Pardo and W. E. Pickett, Phys. Rev. B **78**, 134427 (2008).
[45] A. Droghetti and S. Sanvito, Appl. Phys. Lett. **94**, 252505 (2009).
[46] I. Letard, P. Sainctavit, and C. Deudon, Phys. Chem. Miner. **34**, 113 (2007).
[47] L. Signorini, L. Pasquini, F. Boscherini, E. Bonetti, I. Letard, S. Brice-Profeta, and P. Saincavit, Nucl. Instrum. Methods Phys. Res. B **246**, 20 (2006).
[48] T. C. Kaspar, T. Droubay, S. M. Heald, P. Nachimuthu, C. M. Wang, V. Shutthanandan, C. A. Johnson, D. R. Gamelin, and S. A. Chambers, New J. Phys. **10**, 055010 (2008).
[49] B. Psiuk, J. Sazade, H. Schroeder, H. Haselier, M. Mlynarczyk, R. Waser, and K. Szot, Appl. Phys. A **89**, 451 (2007).
[50] K. Szot, W. Speier, G. Bihlmayer, and R. Waser, Nature Mater. **5**, 312 (2006).
[51] W. A. Ducker, Z. Xe, D. R. Clarke, and J. N. Israelachvili, J. Am. Ceram. Soc. **77**, 437 (1994).
[52] N. H. Nickel and K. Brendel, Phys. Rev. B **68**, 193303 (2003).